

# Reflection and transmission of bottom simulating reflectors in gas hydrate-bearing sediments: Two-phase media models

Ma Jiqiang<sup>†</sup> and Geng Jianhua<sup>†</sup>

**Abstract:** The bottom simulating reflector (BSR) in gas hydrate-bearing sediments is a physical interface which is composed of solid, gas, and liquid and is influenced by temperature and pressure. Deep sea floor sediment is a porous, unconsolidated, fluid saturated media. Therefore, the reflection and transmission coefficients computed by the Zoeppritz equation based on elastic media do not match reality. In this paper, a two-phase media model is applied to study the reflection and transmission at the bottom simulating reflector in order to find an accurate wave propagation energy distribution and the relationship between reflection and transmission and fluid saturation on the BSR. The numerical experiments show that the type I compressional (fast) and shear waves are not sensitive to frequency variation and the velocities change slowly over the whole frequency range. However, type II compressional (slow) waves are more sensitive to frequency variation and the velocities change over a large range. We find that reflection and transmission coefficients change with the amount of hydrate and free gas. Frequency, pore fluid saturation, and incident angle have different impacts on the reflection and transmission coefficients. We can use these characteristics to estimate gas hydrate saturation or detect lithological variations in the gas hydrate-bearing sediments.

**Keyword:** Gas hydrate, BSR, two-phase media, reflection coefficient, transmission coefficient.

## Introduction

Marine gas hydrate is a new hydrocarbon resource discovered after the 1950's. Most are buried in deep highly porous sea floor sediments. Dominated by sea floor temperature and pressure gradient, the pores at the BSR interface can be filled by fluid or gas hydrate and free gas from dissociated hydrates occurs below the BSR interface. The velocity and density of gas hydrate-bearing layers are different than a free gas bearing layer. The boundary between upper and lower pores containing the different fluids generally appears as a bottom simulating reflector (BSR) on seismic sections.

The AVO (amplitude-versus-offset) technique was

proposed to directly detect gas reservoirs two decades ago. Recent research suggests that the AVO technique is an effective method for studying the BSR characteristics. Based on elastic theories, the Zoeppritz equation or its linear approximations are employed for AVO analysis. By studying the reflection and transmission amplitude changes with offset or incident angle, seismic parameters such as P- and S-wave velocity variations are deduced.

However, natural deep sea floor sediments are saturated by fluids. Seismic wave propagation in a porous media is different than in an elastic media. Zoeppritz equation-based elastic theories don't give the correct relations for reflection and transmission in the high porosity sediments under the deep sea floor. It is better to use two- or multi-phase media theories for

---

Manuscript received by the Editor October 22, 2007; revised manuscript received December 7, 2007.

<sup>†</sup>Key laboratory of Marine Geology, School of Ocean and Earth science, Tongji University, Shanghai 200092, China.

BSR AVO analysis. Biot (1956a; 1956b; 1962) and Biot and Willis (1957) proposed three types of waves propagating in porous media: type I compressional (fast P) waves, type II compressional (slow P) waves, and shear waves. Plona (1980; 1982), Plona and Johnson (1980), and Johnson and Plona (1982) proved the existence of these three types of waves by physical experiments. Based on Biot's theory, Dutta and Ode (1983) calculated the phase velocity and attenuation of the three wave types at low-frequencies. Santos et al. (1992) studied a two-phase media model with frequency attenuation effects caused by pore fluid viscosity and rock permeability. Zhang et al. (2005) studied AVO attributes based on two-phase media theories and used AVO attributes to identify gas hydrate and free gas. If the relationship between seismic velocities and pore fluid saturation, the bridge between seismic and gas hydrate-bearing sediments called the rock physics model, is known, it is possible to use AVO techniques to estimate pore fluid or free gas saturation. At least 20 rock physics models for multi-phase media were proposed since 1928 (Geng and Song, 2004; Liu et al., 1994; Liu et al., 2000; Mou, 1996; Song et al., 2002). These models have been applied to study seismic velocity with respect to solid matrix, pore space, and pore fluid properties. The widely used relations in gas hydrate studies are Dvorkin's equations. Three types of rock physics models can be used to describe deep sea gas hydrate-bearing sediments (Dvorkin and Prasad, 1999): (1) gas hydrate is a part of the liquid suspended in the pore fluid; (2) gas hydrate is a part of the solid matrix, which reduces pore space and enhances the bulk modulus of the solid matrix; and (3) gas hydrate is cemented together with the sediment grains, which also reduces pore space and changes the bulk modulus of solid matrix. No matter which model we choose, it will be convenient for us to combine AVO techniques based on two-phase media theories with rock physics models to study BSR characteristics.

In this paper, two-phase media theories are used to study reflection and transmission at the bottom simulating reflector. Dvorkin's equations are applied to link the solid matrix modulus and grain with mineral components. Numerical experiments suggest seismic wave velocities in gas hydrate- and gas-bearing sediments and reflection and transmission coefficients at the BSR change with seismic wave frequency. We can utilize these characteristics to study the BSR and detect gas hydrate- and gas-bearing sediments.

## Two-phase media theory

Wave propagation theory in porous media was presented by Biot (1956a; 1956b). He studied wave propagation in a porous elastic media saturated by compressible viscous fluid. Assuming that motion of the fluid relative to the solid frame can cause friction, the relative displacement is:

$$\mathbf{W} = \phi(\mathbf{U}_f - \mathbf{U}) \quad (1)$$

where  $\phi$  denotes the effective porosity,  $\mathbf{U}$  and  $\mathbf{U}_f$  are the average displacement vectors of the solid and fluid, respectively.  $\mathbf{W}$  represents the averaged relative fluid displacement per unit volume of bulk material.

Defining  $\boldsymbol{\tau}(\mathbf{U}, \mathbf{W})$  as the total stress tensor,  $\mathbf{P}(\mathbf{U}, \mathbf{W})$  as the fluid pressure tensor, and  $\boldsymbol{\varepsilon}_{ij}(\mathbf{U}, \mathbf{W})$  as the strain tensor in the solid,

$$\varepsilon_{ij}(\mathbf{U}) = \frac{1}{2} \left( \frac{\partial U_i}{\partial x_j} + \frac{\partial U_j}{\partial x_i} \right) \quad (2)$$

then the stress-strain relations can be expressed as:

$$\tau_{ij} = 2\mu\varepsilon_{ij}(\mathbf{U}) + \delta_{ij}(\lambda\nabla \cdot \mathbf{U} + D\nabla \cdot \mathbf{W}), \quad 1 \leq i, j \leq 3 \quad (3a)$$

$$\mathbf{p} = -D\nabla \cdot \mathbf{U} - M\nabla \cdot \mathbf{W} \quad (3b)$$

Let the constant  $\mu$  be the shear modulus of the solid matrix,  $K_s$ ,  $K_f$ ,  $K_m$ , and  $K_c$  are the bulk modulus of solid grains, pore fluid, solid matrix, and saturated rock, respectively. The other rock physical parameters can be written as (Dutta and Ode, 1983; Santos et al., 1990):

$$H_c = \lambda_c + 2\mu = K_c + \frac{4}{3}\mu, \quad (4a)$$

$$K_c = K_s[(K_m + Q)/(K_s + Q)], \quad (4b)$$

$$Q = K_f(K_s - K_m)/\phi(K_s - K_f), \quad (4c)$$

$$D = K_s K_f (K_s - K_m) / [K_f (K_s - K_m) + K_s \phi (K_s - K_f)], \quad \text{and} \quad (4d)$$

$$M = K_s^2 K_f / [K_f (K_s - K_m) + K_s \phi (K_s - K_f)]. \quad (4e)$$

The seismic wave propagation equations in two-phase media can be expressed as:

$$\begin{aligned} \nabla \cdot \boldsymbol{\tau} &= H_c \nabla (\nabla \cdot \mathbf{U}) - \mu \nabla \times (\nabla \times \mathbf{U}) + D \nabla (\nabla \cdot \mathbf{W}) \\ &= \rho \frac{\partial^2 \mathbf{U}}{\partial t^2} + \rho_f \frac{\partial^2 \mathbf{W}}{\partial t^2} \end{aligned} \quad (5a)$$

$$\begin{aligned} -\nabla \mathbf{p} &= D \nabla (\nabla \cdot \mathbf{U}) + M \nabla (\nabla \cdot \mathbf{W}) \\ &= \rho_f \frac{\partial^2 \mathbf{U}}{\partial t^2} + g \frac{\partial^2 \mathbf{W}}{\partial t^2} + b \frac{\partial \mathbf{W}}{\partial t} \end{aligned} \quad (5b)$$

where  $\rho$  and  $\rho_f$  are the solid matrix density and fluid density.  $g$  and  $b$  (Dutta and Ode, 1983; Berryman, 1980; 1982) can be calculated as follows:

$$g = S\rho_f / \varphi, \quad (6a)$$

$$b = \eta / k, \quad (6b)$$

where  $S$  is the known structure factor,  $\eta$  is the fluid viscosity, and  $k$  is the rock permeability.

Referring to the method for separating P-waves from S-waves in elastic media, we apply divergence and rotation to equation (5) to get P- and S-wave propagation velocities in two-phase media. Based on Santos's method (1992), P- and S-wave-number vectors can be obtained using the following equations:

$$[MH_c - D^2]q^4 + \{\omega^2[2\rho_f D - gH_c - \rho M] + \omega^4[\rho g - \rho_f^2] - i\omega^3 \rho b\} = 0. \quad (7)$$

$$q_s = \frac{\omega^2}{\mu} \left( \rho - \frac{\rho_f^2}{g - ib/\omega} \right). \quad (8)$$

where  $q$  is the compressional wave-number vector and  $q_s$  is the shear wave-number vector. By solving equation (7) and equation (8), P- and S-wave velocities and attenuations can be obtained. The negative imaginary parts of the roots represent attenuations. The real parts of the roots represent wave velocities.  $q_1$  and  $q_2$  correspond to type I and II compressional wave-numbers, respectively.

P- or S-wave phase velocity  $v_j$  and attenuation  $\xi_j$  are given by the formulas

$$v_j = \omega / |\text{Re}(q_j)|, \quad (9a)$$

$$\xi_j = 2\pi \times 8.685889 \text{Im}(q_j) / |\text{Re}(q_j)|. \quad (9b)$$

Because displacement and stress are continuous at the reflector in two-phase media, Santos gave the following equations for calculating reflection and transmission coefficients:

$$\alpha_{r1}C_{r1} + \alpha_{r2}C_{r2} - \beta_{rs}C_{rs} - \alpha_{t1}C_{t1} - \alpha_{t2}C_{t2} + \beta_{ts}C_{ts} = -\alpha_{i2}, \quad (10a)$$

$$\beta_{r1}C_{r1} + \beta_{r2}C_{r2} + \alpha_{rs}C_{rs} - \beta_{t1}C_{t1} - \beta_{t2}C_{t2} - \alpha_{ts}C_{ts} = -\beta_{i2}, \quad (10b)$$

$$\sigma_{r1}C_{r1} + \sigma_{r2}C_{r2} - \sigma_{rs}C_{rs} - \sigma_{t1}C_{t1} - \sigma_{t2}C_{t2} - \sigma_{ts}C_{ts} = -\sigma_{i2}, \quad (10c)$$

$$[\alpha_{r1}\beta_{r1}C_{r1} + \alpha_{r2}\beta_{r2}C_{r2} - \frac{1}{2}(\beta_{rs}^2 - \alpha_{rs}^2)C_{rs}] \mu^{(1)} - [\alpha_{t1}\beta_{t1}C_{t1} + \alpha_{t2}\beta_{t2}C_{t2} - \frac{1}{2}(\beta_{ts}^2 - \alpha_{ts}^2)C_{ts}] \mu^{(2)} = -\alpha_{i2}\beta_{i2}\mu^{(1)} \quad (10d)$$

$$\delta_{r1}C_{r1} + \delta_{r2}C_{r2} - \delta_{t1}C_{t1} - \delta_{t2}C_{t2} = -\delta_{i2}, \quad (10e)$$

$$\beta_{r1}\gamma_{r1}C_{r1} + \beta_{r2}\gamma_{r2}C_{r2} + \alpha_{rs}\gamma_{rs}C_{rs} - \beta_{t1}\gamma_{t1}C_{t1} - \beta_{t2}\gamma_{t2}C_{t2} - \alpha_{ts}\gamma_{ts}C_{ts} = -\beta_{i2}\gamma_{i2}, \quad (10f)$$

where suffixes 1, 2, and s represent type I compressional, type II compressional, and shear waves, respectively. The suffix r and t represents reflected and transmitted waves.

If  $l = r$ ,  $C_{lj}$  is a reflection coefficient and if  $l = t$ ,  $C_{lj}$  is a transmission coefficient, then the coefficients of the system (10) are given by

$$\beta_{rj} = -\sqrt{q_{rj}^2 - \alpha_{i2}^2}, \quad (11a)$$

$$\beta_{tj} = \sqrt{q_{tj}^2 - \alpha_{i2}^2}, \quad j = 1, 2, s \quad (11b)$$

$$\sigma_{rj} = -H_c^{(1)}q_{rj}^2 - D^{(1)}q_{rj}^2\gamma_{rj} + 2\mu^{(1)}\alpha_{rj}^2, \quad (11c)$$

$$\sigma_{tj} = -H_c^{(2)}q_{tj}^2 - D^{(2)}q_{tj}^2\gamma_{tj} + 2\mu^{(2)}\alpha_{tj}^2, \quad (11d)$$

$$\delta_{rj} = (D^{(1)} + M^{(1)}\gamma_{rj})q_{rj}^2, \quad (11e)$$

$$\delta_{tj} = (D^{(2)} + M^{(2)}\gamma_{tj})q_{tj}^2, \quad j = 1, 2 \quad (11f)$$

$$\sigma_{rs} = 2\mu^{(1)}\alpha_{rs}\beta_{rs}, \sigma_{ts} = 2\mu^{(2)}\alpha_{ts}\beta_{ts}, \quad (11g)$$

where  $q_{i2}$  is the incident wave-number vector,  $q_{ij}$ ,  $j = 1, 2, s$  stands for the reflection wave-number vector, and  $q_{ij}$ ,  $j = 1, 2, s$  stands for the transmission wave-number vector.

## AVA characteristics of gas hydrates at the BSR

### Velocity and attenuation

According to ODP 204 Leg core and log data, the mineral components of sediments under the seafloor are relatively stable, mainly including clay, calcite, and quartz (Underwood and Torres, 2005), with porosity varying from 40% to 80% with an average porosity of 50%. We build a gas hydrate sediment model assuming that the BSR is a plane interface and the sediment matrix is made up of clay, quartz, and calcite with 50% Porosity. Above the BSR we have a 20% gas hydrate-filled pore space and below the BSR a 2% free gas-filled pore space. All the parameters used are listed in Table 1.

Reflection and transmission of bottom simulating reflectors

Table 1 Modulus parameters and component of sediments

component	clay	quartz	calcite	Gas hydrates	Gas
Bulk modulus K(Gpa)	20.9	36	76.8	5.6	0.1
Shear modulus G(Gpa)	6.85	45	32	2.4	0
Density(g/cm <sup>3</sup> )	2.58	2.65	2.71	0.9	0.235
Volume ratio	40% (to solid matrix)	20% (to solid matrix)	40% (to solid matrix)	20% (to pore space)	2% (to pore space)

With equation (4) and Table 1, we can get the parameters in equations (10) and (11). In equation (4), we use the type I gas hydrate model presented by Dvorkin and Prasad (1999), i.e., the gas hydrate is regarded as one part of the fluid,  $K_f$  is obtained by Hill

equation (Zhang et al., 2005), and  $K_m$  by Dvorkin and Nur (1996).

With equations (7), (8), and (9), velocities and attenuations can be resolved and the results are shown in Figures.1 and 2:

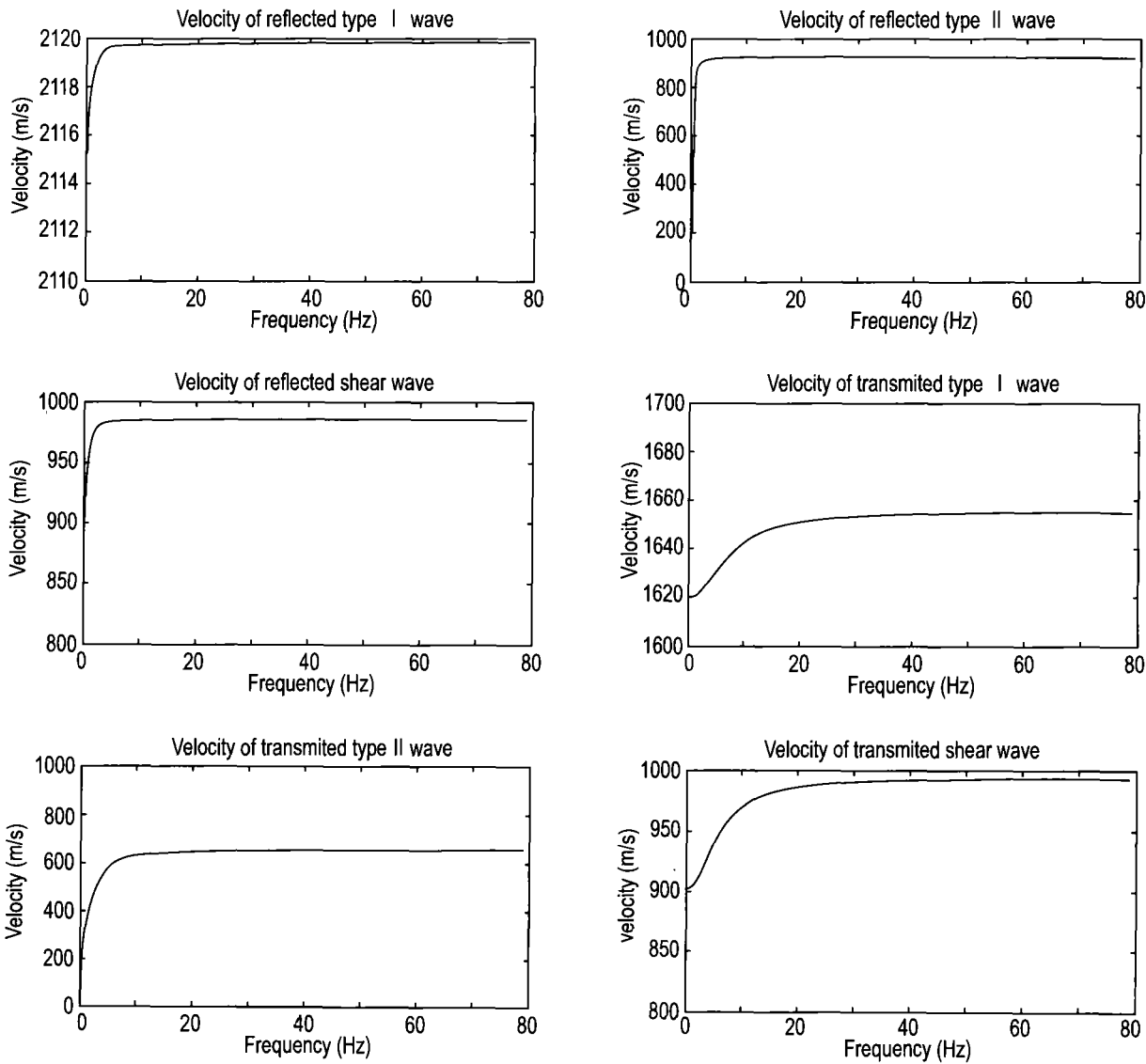


Fig.1 Velocities in the two-phase media from Table 1.

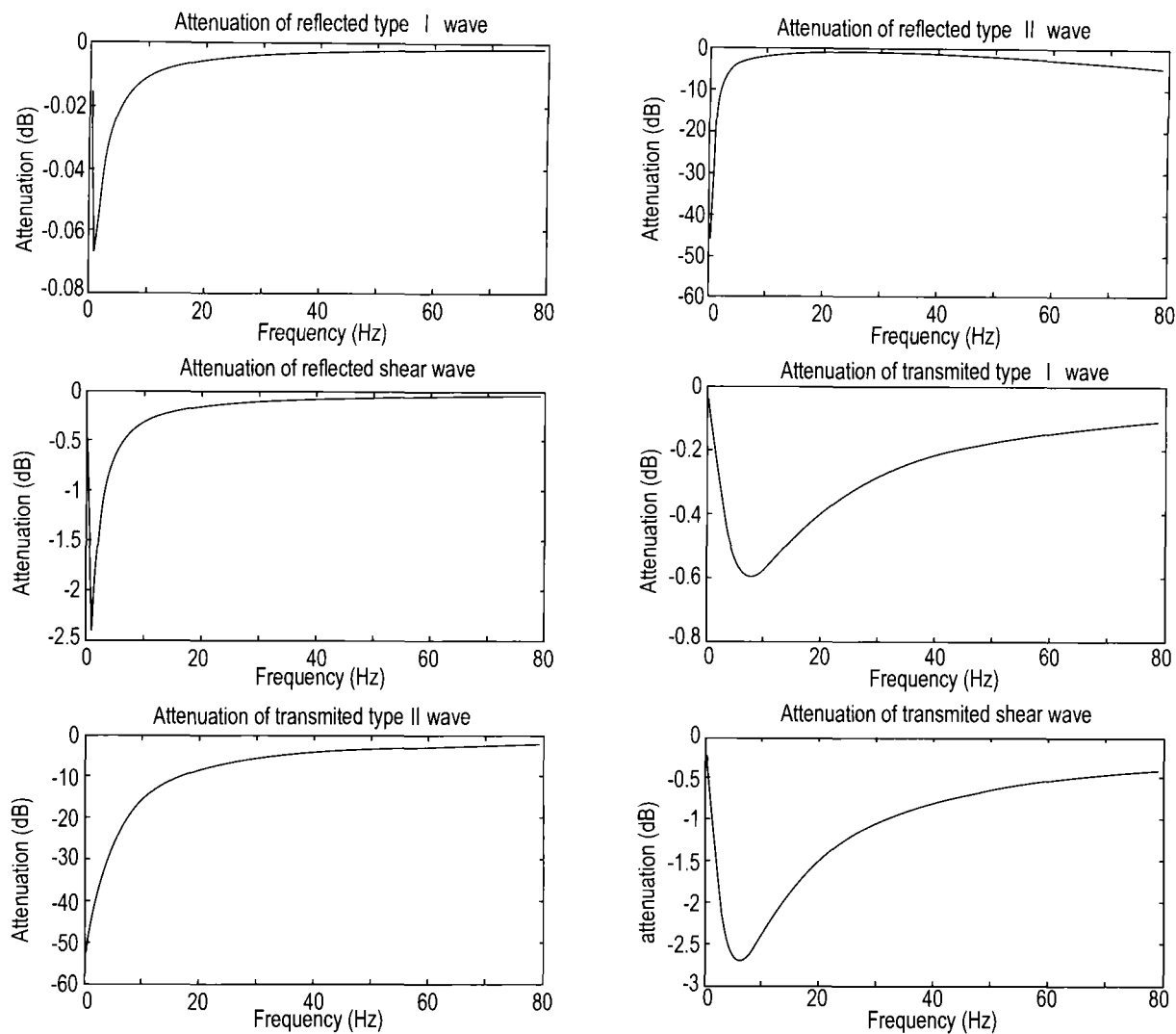


Fig.2 Attenuation coefficients in the two-phase media from Table 1.

From Figures (1) and (2) we can see that the type I compressional and shear waves exhibit little attenuation over the frequency range and the attenuation tends to zero at very low and high frequencies.

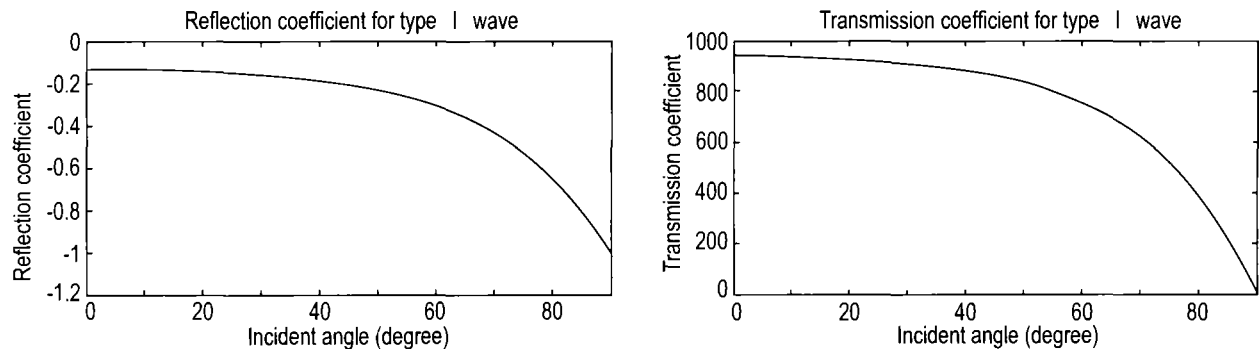
The type II compressional wave is a diffusion-type wave and its attenuation is high. Its velocity tends to zero when the frequency approaches zero and the corresponding attenuation coefficient is  $\xi_2 = -54.575 \text{ dB/Hz}\cdot\text{s}$ . At higher frequencies its attenuation tends to zero. However, the velocity changes with attenuation and as the attenuation approaches a flat line the velocity

approaches a constant.

Reflection and transmission characteristics

Take a type I compressional wave as the incident wave. For the BSR model it is not necessary to consider critical incidence. Using equation (10) we can compute the reflection and transmission coefficients at the BSR.

In Figure 3, we find that at an incidence angle of 90 degrees, the coefficients of type II compressional and shear waves are equal to zero, while the type I compressional wave is completely reflected. As the



### Reflection and transmission of bottom simulating reflectors

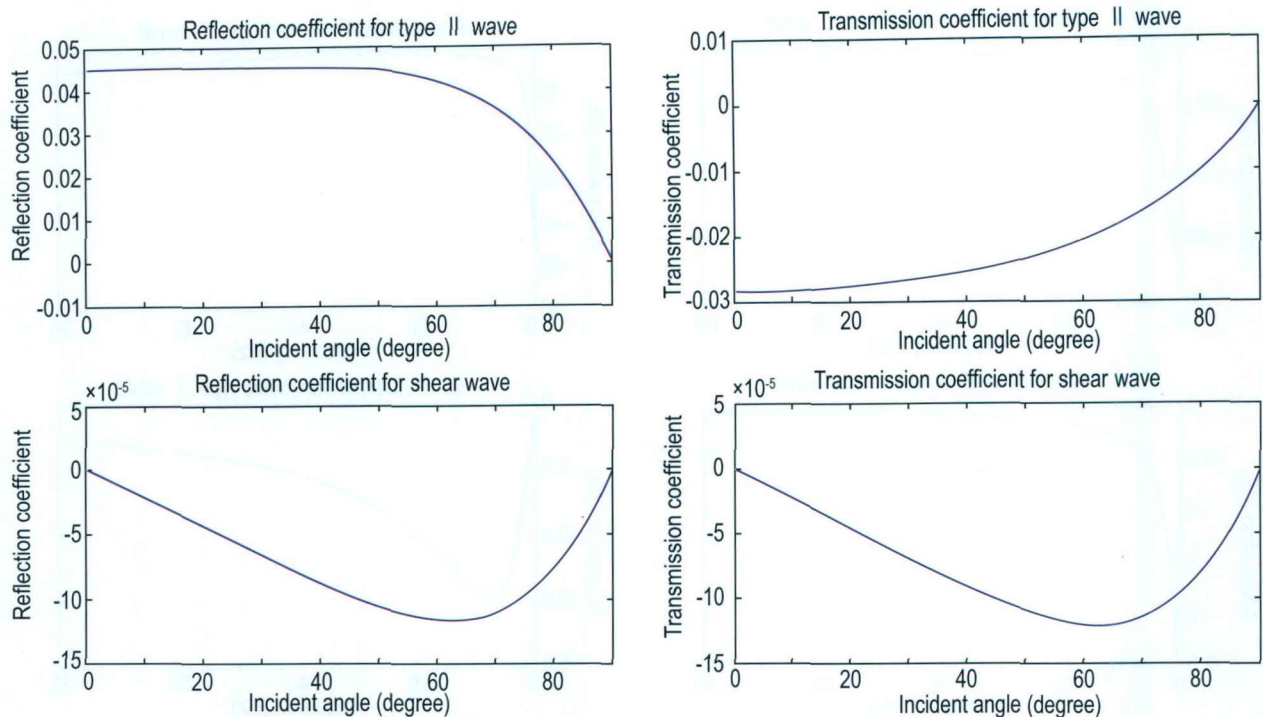
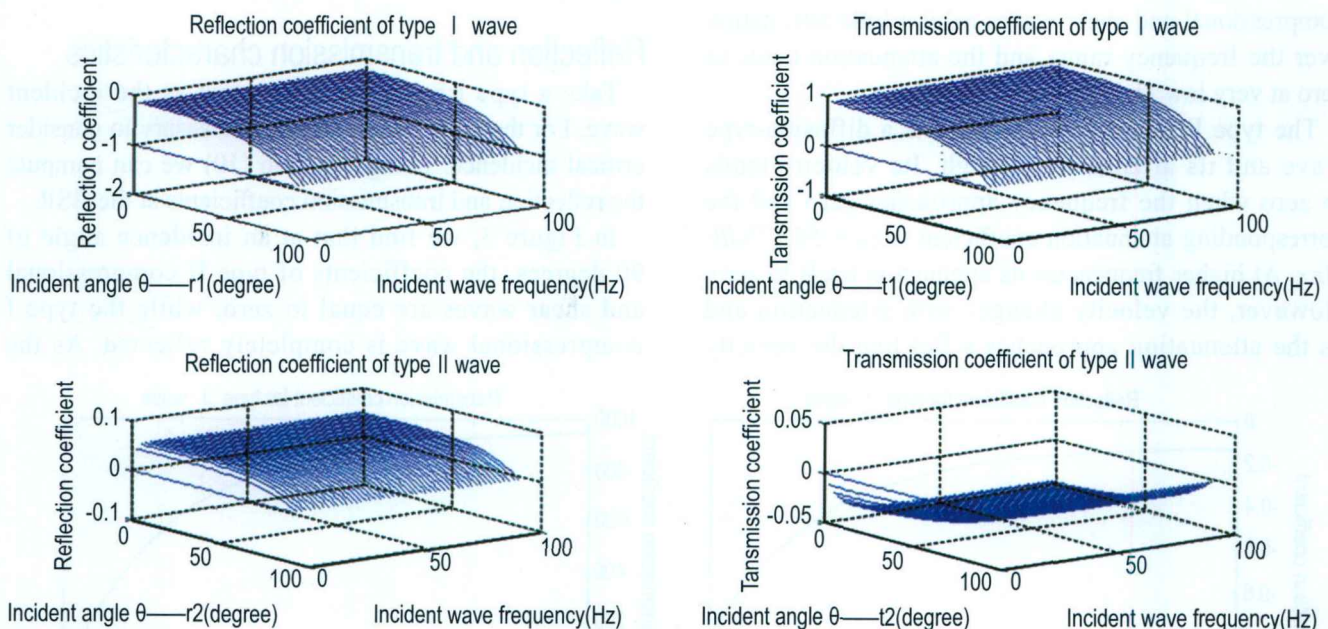


Fig.3 Reflection and transmission coefficients at the BSR.

incident angle changes, the changes in reflection and transmission coefficients of all three wave types are significant.

Figure 4 shows the variations of reflection and transmission coefficients with angle and frequency at the two-phase media interface. Most change in reflection and transmission coefficients occurs at low frequencies and they approach constant values at high

frequencies. This behavior is similar to the attenuation responses seen in Figure 2. However, the overall magnitude of the coefficients of the three wave types are significantly different with type I compressional waves having the largest magnitude, type II compressional waves roughly 10 percent smaller, and shear wave magnitude approximately 100 times smaller than type I compressional waves.





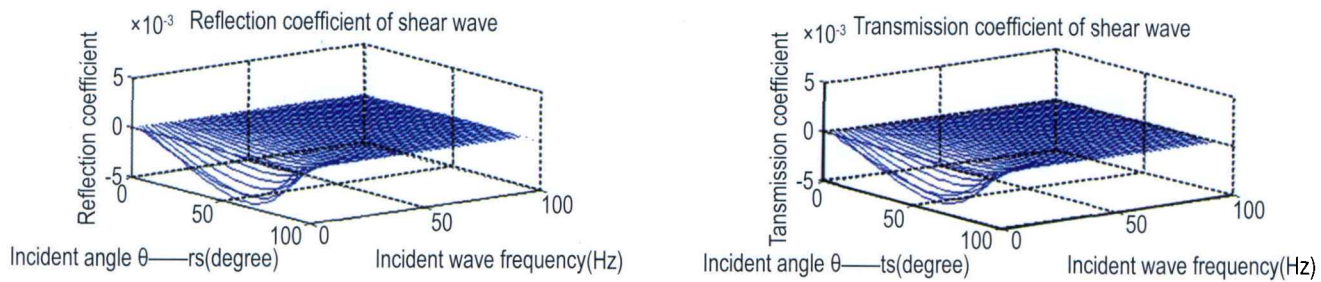


Fig.4 Relationships between reflection and transmission coefficients, angle, and frequency.

Figure 5 shows a slice of Figure 4 which shows the relationships between the reflection and transmission

coefficients and frequency at a 30 degree incidence angle.

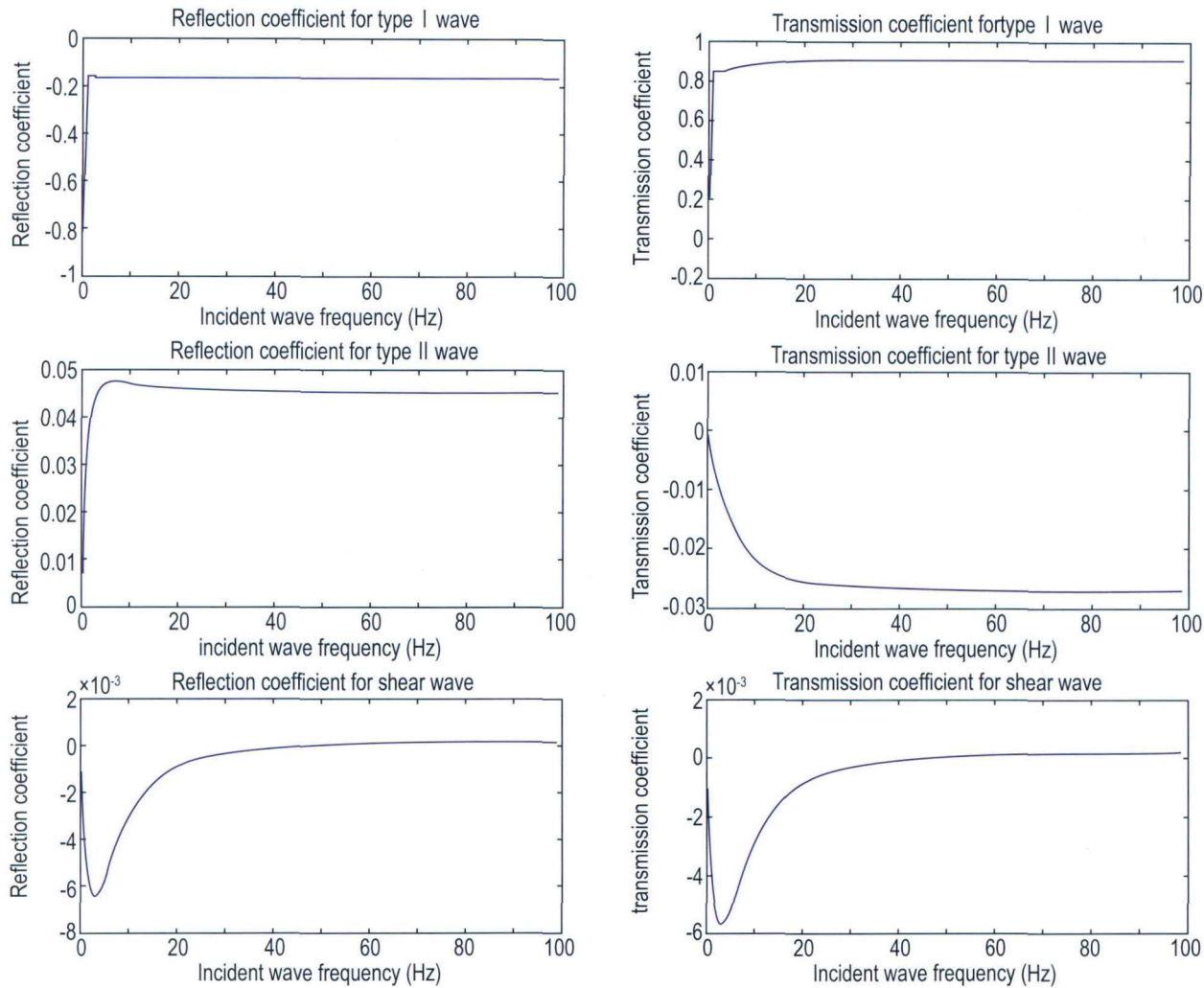


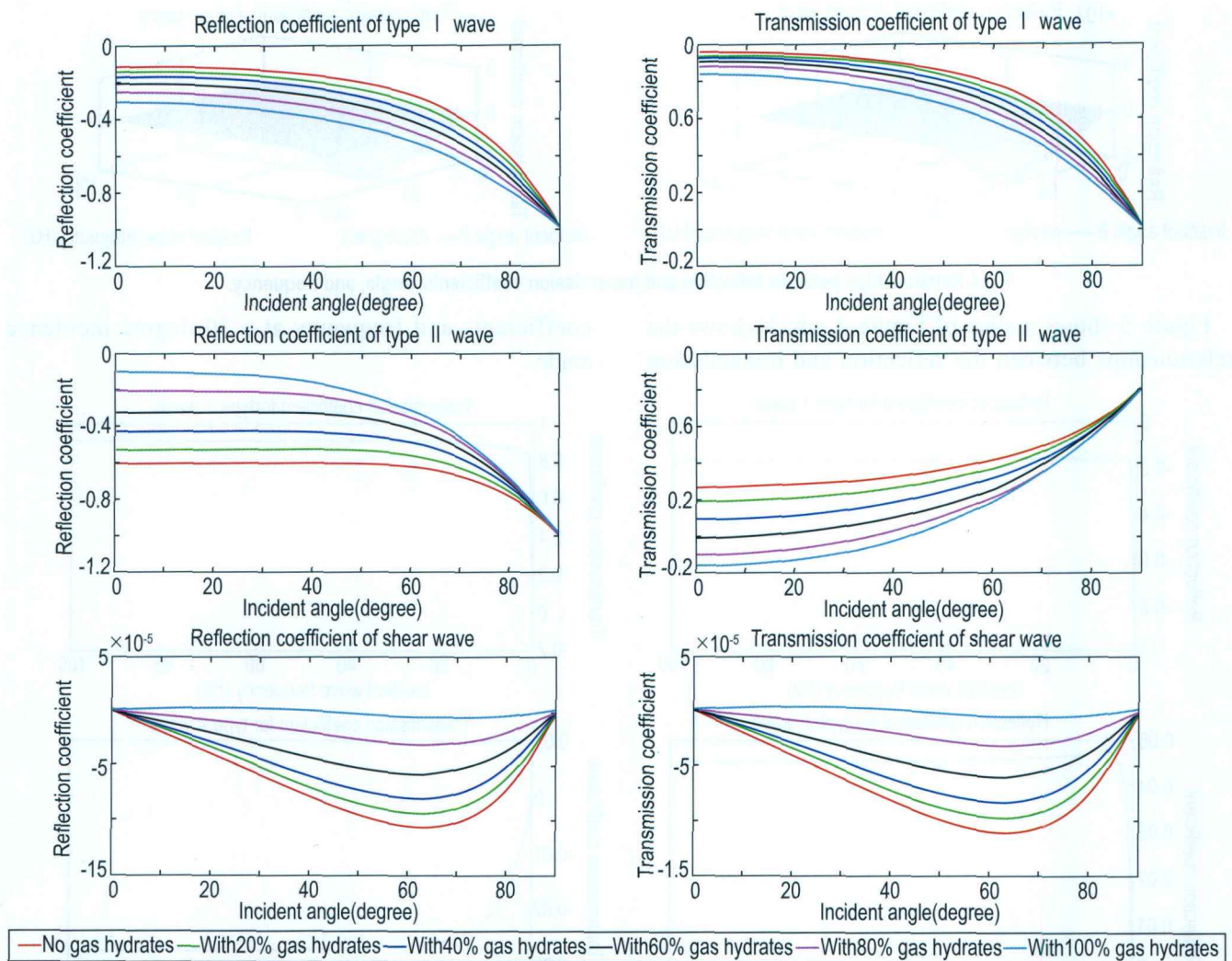
Fig.5 Relationship between reflection and transmission coefficients and frequency when the incidence angle is equal to 30 degrees.

The next experiments study how variations of gas hydrate saturation and free gas change the reflection and transmission coefficients. First, we set the free gas saturation at 2% and vary the gas hydrate saturation in the layer above the BSR from 0 to 100%. The numerical results shown in Figure 6 indicate that as gas hydrate saturation increases, the reflection and transmission coefficients of type I waves decrease, but the corresponding coefficients of type II waves increase. That means fluid viscosity and rock permeability

directly influence the type II waves. Because we take the gas hydrate as a part of the fluid in equation (4), the reflection and transmission coefficients of shear waves decrease as gas hydrate saturation increases.

Second, we keep the amount of gas hydrate in the layer above the BSR set to a constant 20% and vary the free gas amount in the layer below the BSR from 0 to 100%. We will study how the free gas saturation variations will impact the reflection and transmission coefficients at the BSR. The computational results are shown in Figure 7. We

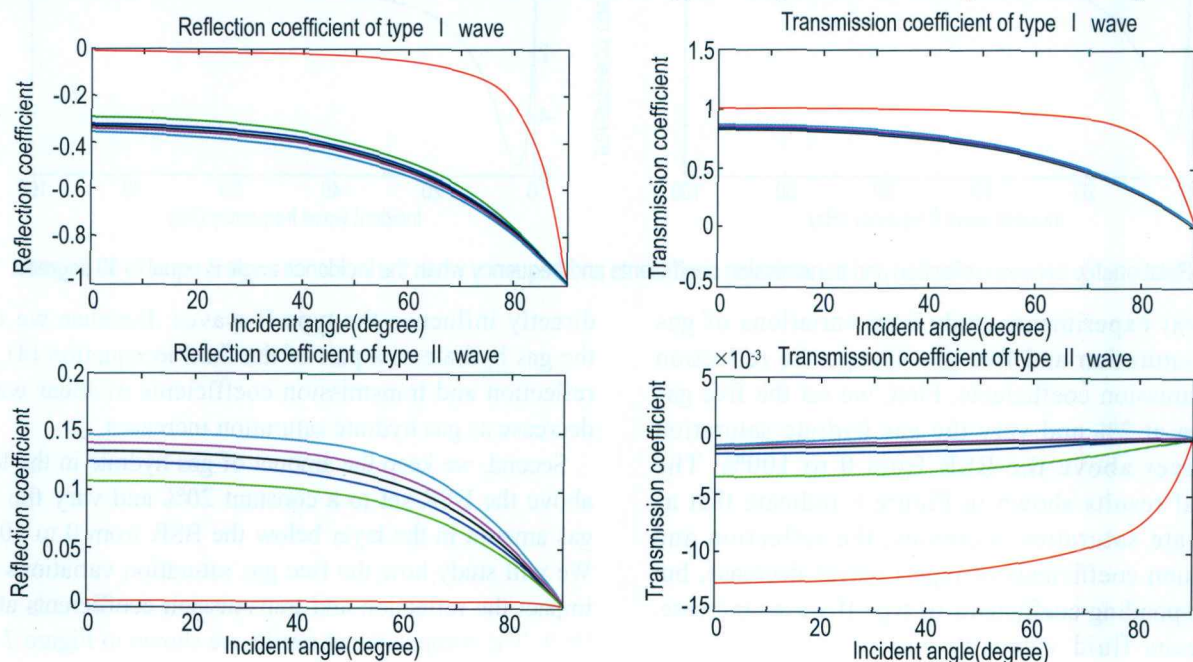
## Reflection and transmission of bottom simulating reflectors



**Fig.6 Reflection and transmission coefficients change with variation of gas hydrate saturation.**

find that free gas saturation variations have small affects on reflection and transmission of shear waves but have a large effect on compressional wave reflection and transmission

coefficients. In other words, P-waves are more sensitive to free gas and we can use the two-phase media model and Type I compressional velocity to detect free gas.





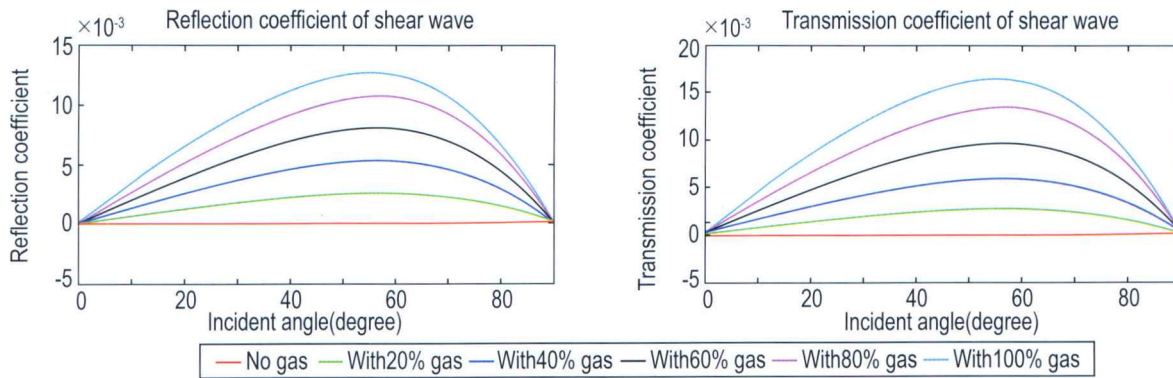


Fig.7 Reflection and transmission coefficient changes with of free gas saturation variations.

## Conclusions

Based on the two-phase model and numerical experiments, we studied the reflection and transmission characteristics of the BSR and we conclude:

1. For gas hydrate bearing layers, type I compressional and shear waves exhibit very little attenuation over the normal range of seismic frequencies and the attenuation tends to zero for low and high frequencies. However, the type II compressional wave exhibits very high attenuation over a wide range of frequencies.
2. The variations of gas hydrate or free gas saturations influence the reflection and transmission coefficients of all three wave types. When gas hydrate saturation changes, the reflection and transmission coefficients of all three wave types also change and the trends of these coefficient curves are almost the same. The free gas curves for different saturations are also nearly the same except for the case with no free gas in the media. From Figures 6 and 7 we find that P-wave reflection and transmission coefficients are more sensitive to free gas saturation. We can use these characteristics to detect free gas and estimate gas saturation, i.e., we can use the AVA characteristics at the BSR to find gas hydrates.
3. All the experiments are based on forward modeling. In theoretical data, the type II compressional waves can be observed, although it is difficult to get any information about type II waves in real data. However, it is still of great value for theoretical research since we can observe them in well logs at short distances.

## Acknowledgements

We thank Key laboratory of Marine Geology, School of Ocean and Earth science, Tongji University for permission to show the data. This research is supported

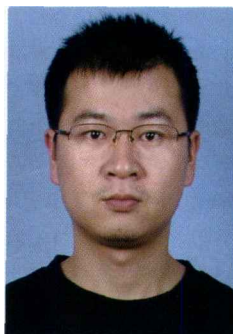
by Program for New Century Excellent Talents in University. Comments by anonymous reviewers helped to improve the original manuscript.

## Reference

- Berryman, J. G., 1980, Confirmation of Biot's theory: *Appl. Phys. Lett.*, **37**, 382 – 384.
- Berryman, J. G., 1982, Elastic waves in fluid-saturated porous media. Macroscopic properties of disordered media: *Lecture Notes in Physics*. **154**, 39 – 49.
- Biot, M. A., 1956a, Theory of propagation of elastic waves in a fluid saturated porous solid. I. Low frequency range: *Journal of Acoustical Society of America*, **28** (2), 168 – 178.
- Biot, M. A., 1956b, Theory of propagation of elastic waves in a fluid saturated porous solid. II. Higher frequency range: *Journal of Acoustical Society of America*, **28** (2), 179 – 191.
- Biot, M. A., 1962, Mechanics of deformation and acoustic propagation in porous media: *J. Appl. Phys.*, **33**, 1482 – 1498.
- Biot, M. A., and Willis, D. G., 1957, The elastic coefficients of the theory of consolidation: *J. Appl. Mech.*, **24**, 594 – 601.
- Dutta, N. C., and Ode, H., 1983, Seismic reflections from a gas-water contact: *Geophysics*, **48**, 148 - 162.
- Dvorkin, J., and Nur, A., 1996, Elasticity of high-porosity sandstones: theory for two North Sea datasets: *Geophysics*, **61**, 1363 – 1370.
- Dvorkin J., and Prasad, M., 1999, Elasticity of marine sediments: rock physics modeling: *Geophysical Research Letters*, **26** (12), 1781-1784.
- Geng, J. H., and Song, H. B., 2004, Iced energy: gas hydrate: *Science (in Chinese)*, **56** (4), 15 – 18.
- Johnson, D. L., and Plona, T. J., 1982, Acoustic slow waves and the consolidation transition: *Journal of*

- Acoustical Society of America, **72**, 556 – 565.
- Liu, Y., Li, C. C., and Mou, Y. G., 2000, Research on propagation properties of elastic wave in two-phase anisotropic media: *Acta Seismologica Sinica* (in Chinese), **43** (5), 691 – 698.
- Liu, Y. B., Li, Y. M., and Wu, R. S., 1994, Research on seismic wave propagation in transversely isotropic porous medium: *Chinese J. Geophys.* (in Chinese), **37** (4), 499 – 513.
- Mou, Y. G., 1996, *Reservoir geophysics*: Petroleum Industry Press, Beijing, China.
- Plona, T. J., 1980, Observation of a second bulk compressional wave in a porous medium at ultrasonic frequencies: *Appl. Phys. Lett.*, **36**, 259 – 261.
- Plona, T. J., 1982, Acoustics of fluid-saturated porous media: *Ultrason. Symp.*, IEEE, **20**, 1044 – 1048.
- Plona, T. J., and Johnson, D. L., 1980, Experimental study of the two bulk compressional modes in water-saturated porous structure: *Ultrason. Symp.*, IEEE, **18**, 868 – 872.
- Santos, J. E., Corbero, J. M., and Douglas, J. Jr., 1990, Static and dynamic behavior of a porous solid saturated by a two-phase fluid: *Journal of Acoustical Society of America*, **87**, 1428 – 1438.
- Santos, J. E., Corbero, J. M., Ravazzoli, C. L., and Hensley, J. L., 1992, Reflection and transmission coefficients in fluid-saturated porous media: *Journal of Acoustical Society of America*, **91** (4), 1911 – 1923.
- Song, H. B., Osamu, M., Yang, S. X., Wu, N. Y., Jiang, W. W., and Hao, T. Y., 2002, Physical property models of gas hydrate-bearing sediments and AVA character of bottom simulating reflector: *Chinese J. Geophys.* (in Chinese), **45** (4), 546 – 556.
- Underwood, M., and Torres, M., 2005, Data report: Composition of clay minerals from hemipelagic sediments at hydrate ridge, Cascadia subduction zone, in Tréhu, A. M., Bohrmann, G., Torres, M. E., and Colwell, F.S., Eds.: *Proceedings of the Ocean Drilling Program, Scientific Results, Volume 204*.
- Zhang, Y. W., Liu, X. W., and Yao, C. L., 2005, Recognition of gas hydrate using AVO-attribute crossplots based on the porous medium theory: *Applied Geophysics*, **2** (1), 7 – 13.

**Ma Jiqiang** graduated from the School of Ocean and Earth Science, Tongji University, in 2006 with his Bachelor's degree. His interests are AVO research and application.



场分析,得到了较好的结果。

关键词: BISQ模型, 三维数值模拟, 交错网格, 双相各向异性介质。

5. 转换波AVO反演速度比和横波反射系数// Converted wave AVO inversion for average velocity ratio and reflection coefficient of shear wave, 魏修成, 陈天胜, 季玉新, *Applied Geophysics*, 2008, 5(1), 35 - 43.

(中国石化石油勘探开发研究院 北京学院路, 100083)

摘要: 本文提出了转换波AVO极值属性,并在储层密度和纵波速度满足Gardner公式的基础上,推导了极值位置和极值振幅与界面两侧速度比平均值和横波反射系数的关系。极值点位置是速度比平均值的函数,且随速度比的增加而减小,转换波AVO曲线的极值是速度比平均值和横波反射系数的函数。针对理论模型,利用幂函数拟合得到较高精度的AVO曲线极值位置和极值振幅,反演得到比较准确的速度比和横波反射系数。得到的横波反射系数剖面比常规转换波叠加剖面更有明确的物理意义,为地质构造解释和转换波层位标定奠定了理论基础。最后把转换波AVO曲线幂函数拟合和极值属性反演纵横波速度比、横波反射系数的方法应用于某地区实际转换波共转换点道集,反演的速度比与纵横波测井计算的速度比较吻合。

关键词: 转换波, AVO, 极值属性, 地震反演, 速度比, 反射系数

6. 低信噪比转换波地震资料静校正// Static corrections for low S/N ratio converted-wave seismic data, 李国发<sup>1,2</sup>, 彭苏萍<sup>1</sup>, *Applied Geophysics*, 2008, 5(1), 44 - 49.

(1. 中国矿业大学资源与安全工程学院地震勘探实验室, 北京, 100083; 2. 中国石油大学CNPC物探重点实验室, 北京102249; )

摘要: 由于转换波具有低速、低信噪比的特点,以及初至拾取和共转换点分选的困难,一些相对成熟的纵波资料静校正方法不能很好地解决转换波静校正问题,转换波静校正问题成为转换波处理取得突破主要技术障碍。为了改进转换波静校正的应用效果,首先利用共检波点叠加静校正方法,通过改善共检波点叠加剖面的质量对检波点进行初始静校正,然后利用叠加能量最大静校正方法,通过改善共转换点剖面的质量对检波点进行更精细的静校正,最后对共转换点道集进行非地表一致性剩余时差校正,增强不同深度反

射信号的叠加质量。通过三种静校正方法的联合应用,较好地解决了转换波地震资料的静校正问题。

关键词: 转换波, 静校正, 共检波点叠加最大叠加能量, 非地表一致性

7. 转换波四参数速度分析方法在k71地区的应用// Four-parameter velocity analysis and its applications to the Ken-71 area converted-wave data, 石建新, *Applied Geophysics*, 2008, 5(1), 50 - 56.

(1. 中国石油大学(华东)地球资源与信息学院;  
2. 中石化胜利油田物探研究院)

摘要: 胜利油田垦71地区多分量地震资料采用微型三分量数字检波器采集,该区上覆地层为砂岩和页岩交互层。由于转换波传播路径的非对称性和各向异性等因素的影响,造成了转换波资料中同相轴的非双曲现象。利用传统的基于各向同性理论进行速度分析,动校正时无法把同相轴拉平。本文使用转换波四参数理论估算非双曲效应,进行转换波速度分析和数据处理。这四个参数包括转换波叠加速度( $V_{c2}$ )、垂直速度比( $y_0$ )、等效速度比( $y_{eff}$ )和转换波各向异性系数( $x_{eff}$ )。此方法利用不同偏移距的动校正信息来估算不同的参数,确保了同相轴的同相叠加。将该方法应用于胜利油田垦71地区数字检波器三维转换波资料的处理中取得了较好的应用效果,提高了转换波资料的成像质量,改善了纵波—转换波的对层分析。

关键词: 转换波, 四参数速度分析, 叠前偏移

8. 天然气水合物似海底反射层(BSR)AVA特征: 双相介质模型// Reflection and transmission on bottom simulating reflector in gas hydrate bearing sediments: Two-phase media models, 麻纪强, 耿建华 *Applied Geophysics*, 2005, 5(1), 57 - 66.

(同济大学海洋与地球科学学院 海洋地质国家重点实验室, 中国上海 200092)

摘要: 天然气水合物似海底反射层是一个由固体、气体和液体等多相介质组成、受温度和压力影响的物理分界面,所以基于弹性介质Zoeppritz方程计算的反射和透射系数都不能满足实际的分析需要,因此需要研究多相介质分界面上的反射和透射特征。但是由于多相介质理论的复杂性,在研究中可以将多相介质近似看作是双相介质,也就是说可以将含天然气水合物沉积地层简化为双相介质,来研究波在其BSR分界面上

随频率和入射角度的变化所反映出的反射和透射的特征,并且改变BSR上下层介质中水合物含量和游离气含量,进一步研究波在介质分界面上的反射和透射特征与流体饱和度的关系。对模型计算发现第一类纵波和横波对频率的变化不敏感,速度改变不大;而第二类纵波受频率的影响较大,速度变化范围较大;随着水合物和游离气含量的变化,各种反射和透射波都会随之改变,变化的范围和幅度说明了波对介质组分变化的敏感性。

**关键词:** 天然气水合物, 似海底反射层, 双相介质、反射系数, 透射系数, 饱和度

9. 地球物理技术在天然气水合物预测中的应用//  
Applications of seismic techniques to gas hydrates prediction,  
刘彦君<sup>1</sup>, 刘喜武<sup>2</sup>, 刘大锰<sup>1</sup>, 王燕津<sup>3</sup>, 赵迎新<sup>3</sup>,  
Applied Geophysics, 2008, 5(1), 67 - 73

(1中国地质大学, 北京学院路 100083; 2中国海洋大学, 山东 青岛 266100; 3 吉林油田, 吉林 松原 138000)

**摘要:** 本文基于天然气水合物发育区特有的构造沉积特征对各种地球物理响应的敏感性,研究了地震属性、AVO分析、陡倾角地层反转速度场建立、及伪井约束波阻抗反演等地震技术在天然气水合物预测中的应用及其效果。通过多信息联合分析与融合策略,优化集成有效地球物理技术,形成一套可靠的天然气水合物探测技术与流程。实际表明:综合分析反射强度、瞬时相位、层速度、相对波阻抗、绝对波阻抗、及AVO截距剖面等特征资料是识别天然气水合物底界似海底反射(BSR)的有效手段;综合应用地震、相对波阻抗、绝对波阻抗、层速度等剖面的特征可提高天然气水合物识别的有效性;而瞬时频率、能量半衰时、层速度、AVO截距、AVO乘积、AVO流体因子等剖面特征的有效组合能更准确有效地识别BSR以下的游离气。文中

所总结的一套预测天然气水合物的优化组合地球物理技术在我国南海海域中已取得良好效果。

**关键词:** 地震属性, 特殊处理, 天然气水合物, BSR, 预测

10. 利用大地电磁资料对玄武岩成像的可行性//  
Feasibility of using magnetotelluric for sub-basalt imaging at Kutch, India, Dhananjai Pande<sup>y1,3</sup>, Lucy MacGregor<sup>2</sup>, Martin Sinha<sup>3</sup>, Satish Singh<sup>4</sup>, Applied Geophysics, 2008, 5(1), 74 - 82.

(1.Bullard Laboratories, Madingley Road, University of Cambridge, Cambridge, UK, CB3 0EZ; Presently at National Centre for Antarctic and Ocean Research, Goa; 2. Offshore Hydrocarbon Mapping Plc., Aberdeen, UK, AB23 8GD; 3. SOES, National Oceanography Centre, Southampton, UK, SO14 3ZH; 4. Laboratoire de Géosciences Marines, IPG Paris 4 Place Jussieu, 75252 Paris Cedex 05, France)

**摘要:** 磁大地电流法(MT)已成为有助于地下盐和地下玄武岩地震成像的有利方法之一。本文印度卡奇地区(这个地区玄武岩覆盖了中生代沉积岩)。并讨论了利用MT方法作为这样地质背景地区勘探工具的可能性。我们的结果突出了由侵入薄层玄武岩引起的磁大地电流响应的差别。本文讨论的关键问题是在这样的地质背景条件下MT方法能够或不能提供什么。首先我们利用了具有代表性的电阻率—深度模型和研究区的井资料计算了视电阻率和相位响应曲线,然后对这些结果的对比分析,评估了利用MT对Kachchh地区地下火成岩沉积成像的合理性。最后,通过对这个地区野外观测的MT资料一维反演证实了我们的讨论。

**关键词:** 地下玄武岩成像, 德干圈闭, 卡奇, 磁大地电流。